

# Energy dissipation and switching delay in stress-induced switching of multiferroic devices in the presence of thermal fluctuations

Kuntal Roy,<sup>1, a)</sup> Supriyo Bandyopadhyay,<sup>1</sup> and Jayasimha Atulasimha<sup>2</sup>

<sup>1)</sup> *Department of Electrical and Computer Engineering, Virginia Commonwealth University, Richmond, VA 23284, USA*

<sup>2)</sup> *Department of Mechanical and Nuclear Engineering, Virginia Commonwealth University, Richmond, VA 23284, USA*

(Dated: 5 April 2018)

Switching the magnetization of a shape-anisotropic 2-phase multiferroic nanomagnet with voltage-generated stress is known to dissipate very little energy ( $< 1$  aJ for a switching time of  $\sim 0.5$  ns) at 0 K temperature. Here, we show by solving the stochastic Landau-Lifshitz-Gilbert equation that switching can be carried out with  $\sim 100\%$  probability in less than 1 ns while dissipating less than 2 aJ at *room temperature*. This makes nanomagnetic logic and memory systems, predicated on stress-induced magnetic reversal, one of the most energy-efficient computing hardware extant. We also study the dependence of energy dissipation, switching delay, and the critical stress needed to switch, on the rate at which stress is ramped up or down.

PACS numbers: 85.75.Ff, 75.85.+t, 75.78.Fg, 81.70.Pg, 85.40.Bh

Keywords: Nanomagnets, multiferroic, LLG equation, thermal analysis, energy-efficient design

## I. INTRODUCTION

Shape-anisotropic multiferroic nanomagnets, consisting of magnetostrictive layers elastically coupled with piezoelectric layers<sup>1,2</sup>, have emerged as attractive storage and switching elements for non-volatile memory and logic systems since they are potentially very energy-efficient. Their magnetizations can be switched in less than 1 nanosecond with energy dissipation less than 1 aJ, when no thermal noise is present<sup>3,4</sup>. This has led to multiple logic proposals incorporating these systems<sup>5-7</sup>. The magnetization of the magnet has two (mutually anti-parallel) stable states along the easy axis that encode the binary bits 0 and 1. The magnetization is flipped from one stable state to the other by applying a tiny voltage of few tens of millivolts across the piezoelectric layer while constraining the magnetostrictive layer from expanding or contracting along its in-plane hard-axis. The voltage generates a strain in the piezoelectric layer, which is then transferred to the magnetostrictive layer. That produces a uniaxial stress in the magnetostrictive layer along its easy-axis and rotates the magnetization towards the in-plane hard axis as long as the product of the stress and the magnetostrictive coefficient is *negative*. Large angle rotations by this method have been demonstrated in recent experiments<sup>8</sup>, although not in nanoscale.

In this paper, we have studied the switching dynamics of a single-domain magnetostrictive nanomagnet, subjected to uniaxial stress, in the presence of thermal fluctuations. The dynamics is governed by the stochastic Landau-Lifshitz-Gilbert (LLG) equation<sup>9,10</sup> that describes the time-evolution of the magnetization vector's orientation under various torques. There are *three*

torques to consider here: torque due to shape anisotropy, torque due to stress, and the torque associated with random thermal fluctuations. With realistic ramp rates (rate at which stress on the magnet is ramped up or down) a magnet can be switched with  $\sim 100\%$  probability with a (thermally averaged) switching delay of  $\sim 0.5$  ns and (thermally averaged) energy dissipation  $\sim 200$   $kT$  at room-temperature. This is very promising for “beyond-Moore’s law” ultra-low-energy computing<sup>11-13</sup>. Our simulation results show the following: (1) a fast ramp and a sufficiently high stress are required to switch the magnet with high probability in the presence of thermal noise, (2) the stress needed to switch with a given probability increases with decreasing ramp rate, (3) if the ramp rate is too slow, then the switching probability may never approach 100% no matter how much stress is applied, (4) the switching probability increases monotonically with stress and saturates at  $\sim 100\%$  when the ramp is fast, but exhibits a non-monotonic dependence on stress when the ramp is slow, and (5) the thermal averages of the switching delay and energy dissipation are nearly independent of the ramp rate if we always switch with the critical stress, which is the minimum value of stress needed to switch with non-zero probability in the presence of noise.

## II. MODEL

### A. Magnetization dynamics of a magnetostrictive nanomagnet in the presence of thermal noise: Solution of the stochastic Landau-Lifshitz-Gilbert equation

Consider an isolated nanomagnet in the shape of an elliptical cylinder whose elliptical cross section lies in the  $y$ - $z$  plane with its major axis aligned along the  $z$ -direction and minor axis along the  $y$ -direction (Fig. 1.) The dimension of the major axis is  $a$ , that of the minor axis is  $b$ ,

<sup>a)</sup> Electronic mail: royk@vcu.edu.

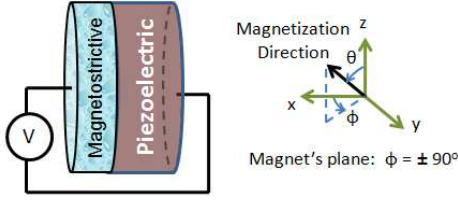


FIG. 1. A two-phase multiferroic nanomagnet in the shape of an elliptical cylinder is stressed with an applied voltage via the  $d_{31}$  coupling in the piezoelectric. Mechanical constraints (not shown) prevent expansion and contraction of the multiferroic along the in-plane hard axis ( $y$ -axis).

and the thickness is  $l$ . The  $z$ -axis is the easy axis, the  $y$ -axis is the in-plane hard axis and the  $x$ -axis is the out-of-plane hard axis. Since  $l \ll b$ , the out-of-plane hard axis is much harder than the in-plane hard axis. Let  $\theta(t)$  be the polar angle and  $\phi(t)$  the azimuthal angle of the magnetization vector.

The total energy of the single-domain, magnetostrictive, polycrystalline nanomagnet, subjected to uniaxial stress along the easy axis (major axis of the ellipse) is the sum of the uniaxial shape anisotropy energy and the uniaxial stress anisotropy energy<sup>14</sup>. The former is given by<sup>14</sup>  $E_{SHA}(t) = (\mu_0/2)M_s^2\Omega N_d(t)$ , where  $M_s$  is the saturation magnetization and  $N_d(t)$  is the demagnetization factor expressed as<sup>14</sup>

$$N_d(t) = N_{d-zz}\cos^2\theta(t) + N_{d-yy}\sin^2\theta(t)\sin^2\phi(t) + N_{d-xx}\sin^2\theta(t)\cos^2\phi(t) \quad (1)$$

with  $N_{d-zz}$ ,  $N_{d-yy}$ , and  $N_{d-xx}$  being the components of the demagnetization factor along the  $z$ -axis,  $y$ -axis, and  $x$ -axis, respectively<sup>15</sup>. These factors depend on the dimensions of the magnet (values of  $a$ ,  $b$  and  $l$ ). We choose these dimensions as  $a = 100$  nm,  $b = 90$  nm and  $l = 6$  nm, which ensures that the magnet has a single domain<sup>16</sup>. These dimensions also determine the shape anisotropy energy barriers. The in-plane barrier  $E_b$ , which is the difference between the shape anisotropy energies when  $\theta = 90^\circ$  and  $\theta = 0^\circ, 180^\circ$  ( $\phi = \pm 90^\circ$ ) determines the static error probability, which is the probability of spontaneous magnetization reversal due to thermal noise. This probability is  $\exp[-E_b/kT]$ . For the dimensions and material chosen,  $E_b = 44$   $kT$  at room temperature, so that the static error probability at room temperature is  $e^{-44}$ .

The stress anisotropy energy is given by<sup>14</sup>  $E_{STA}(t) = -(3/2)\lambda_s\sigma(t)\Omega\cos^2\theta(t)$ , where  $(3/2)\lambda_s$  is the magnetostriction coefficient of the nanomagnet and  $\sigma(t)$  is the stress at an instant of time  $t$ . Note that a positive  $\lambda_s\sigma(t)$  product will favor alignment of the magnetization along the major axis ( $z$ -axis), while a negative  $\lambda_s\sigma(t)$  product will favor alignment along the minor axis ( $y$ -axis), because that will minimize  $E_{STA}(t)$ . In our convention, a compressive stress is negative and tensile stress is positive. Therefore, in a material like Terfenol-D that has

positive  $\lambda_s$ , a compressive stress will favor alignment along the minor axis (in-plane hard axis), and tensile along the major axis (easy axis)<sup>3</sup>.

At any instant of time  $t$ , the total energy of the nanomagnet can be expressed as

$$E(t) = E(\theta(t), \phi(t), \sigma(t)) = B(t)\sin^2\theta(t) + C(t) \quad (2)$$

where

$$B(t) = B_0(t) + B_{stress}(t) \quad (3a)$$

$$B_0(t) = (\mu_0/2)M_s^2\Omega[N_{d-xx}\cos^2\phi(t) + N_{d-yy}\sin^2\phi(t) - N_{d-zz}] \quad (3b)$$

$$B_{stress}(t) = (3/2)\lambda_s\sigma(t)\Omega \quad (3c)$$

$$C(t) = (\mu_0/2)M_s^2\Omega N_{d-zz} - (3/2)\lambda_s\sigma(t)\Omega. \quad (3d)$$

The torque acting on the magnetization per unit volume due to shape and stress anisotropy is

$$\mathbf{T}_E(t) = -\mathbf{n}_m(t) \times \nabla E(\theta(t), \phi(t), \sigma(t)) = -2B(t)\sin\theta(t)\cos\theta(t)\hat{\mathbf{e}}_\phi - B_{0e}(t)\sin\theta(t)\hat{\mathbf{e}}_\theta \quad (4)$$

where  $B_{0e}(t) = (\mu_0/2)M_s^2\Omega(N_{d-xx} - N_{d-yy})\sin(2\phi(t))$ .

The torque due to thermal fluctuations is treated via a random magnetic field  $\mathbf{h}(t)$  and is expressed as

$$\mathbf{h}(t) = h_x(t)\hat{\mathbf{e}}_x + h_y(t)\hat{\mathbf{e}}_y + h_z(t)\hat{\mathbf{e}}_z \quad (5)$$

where  $h_x(t)$ ,  $h_y(t)$ , and  $h_z(t)$  are the three components of the random thermal field  $\mathbf{h}(t)$  in  $x$ -,  $y$ -, and  $z$ -direction, respectively in Cartesian coordinates. We assume the properties of the random field  $\mathbf{h}(t)$  as described in Ref. [10]. Accordingly, the random thermal field can be expressed as

$$h_i(t) = \sqrt{\frac{2\alpha kT}{|\gamma|(1+\alpha^2)M_V\Delta t}} G_{(0,1)}(t) \quad (i = x, y, z) \quad (6)$$

where  $1/\Delta t$  is proportional to the attempt frequency of the thermal field. Consequently,  $\Delta t$  should be the simulation time-step used to simulate switching trajectories in the presence of random thermal torque. The quantity  $G_{(0,1)}(t)$  is a Gaussian distribution with zero mean and unit variance<sup>17</sup>.

The thermal torque can be written as

$$\mathbf{T}_{TH}(t) = M_V \mathbf{n}_m(t) \times \mathbf{h}(t) = P_\theta(t)\hat{\mathbf{e}}_\phi - P_\phi(t)\hat{\mathbf{e}}_\theta \quad (7)$$

where

$$P_\theta(t) = M_V[h_x(t)\cos\theta(t)\cos\phi(t) + h_y(t)\cos\theta(t)\sin\phi(t) - h_z(t)\sin\theta(t)] \quad (8)$$

$$P_\phi(t) = M_V[h_y(t)\cos\phi(t) - h_x(t)\sin\phi(t)]. \quad (9)$$

The magnetization dynamics under the action of the torques  $\mathbf{T}_E(t)$  and  $\mathbf{T}_{TH}(t)$  is described by the stochastic Landau-Lifshitz-Gilbert (LLG) equation as follows.

$$\frac{d\mathbf{n}_m(t)}{dt} - \alpha \left( \mathbf{n}_m(t) \times \frac{d\mathbf{n}_m(t)}{dt} \right) = -\frac{|\gamma|}{M_V} [\mathbf{T}_E(t) + \mathbf{T}_{TH}(t)] \quad (10)$$

where  $\alpha$  is the dimensionless phenomenological Gilbert damping constant,  $\gamma = 2\mu_B\mu_0/\hbar$  is the gyromagnetic ratio for electrons and is equal to  $2.21 \times 10^5$  (rad.m).(A.s) $^{-1}$ ,  $\mu_B$  is the Bohr magneton, and  $M_V = \mu_0 M_s \Omega$ .

From the last equation, we get the following coupled equations for the dynamics of  $\theta(t)$  and  $\phi(t)$ .

$$(1 + \alpha^2) \frac{d\theta(t)}{dt} = \frac{|\gamma|}{M_V} [B_{0e}(t) \sin\theta(t) - 2\alpha B(t) \sin\theta(t) \cos\theta(t) + (\alpha P_\theta + P_\phi)]. \quad (11)$$

$$(1 + \alpha^2) \frac{d\phi(t)}{dt} = \frac{|\gamma|}{M_V} [\alpha B_{0e}(t) + 2B(t) \cos\theta(t) - \sin^{-1}\theta(t) (P_\theta - \alpha P_\phi)]. \quad (\sin\theta \neq 0.) \quad (12)$$

These equations describe the magnetization dynamics, namely the temporal evolution of the magnetization vector's orientation, in the presence of thermal noise.

### B. Fluctuation of magnetization around the easy axis (stable orientation) due to thermal noise

The torque on the magnetization vector due to shape and stress anisotropy vanishes when  $\sin\theta = 0$  [see Equation (4)], i.e. when the magnetization vector is aligned along the easy axis. That is why  $\theta = 0^\circ, 180^\circ$  are called *stagnation points*. Only thermal fluctuations can budge the magnetization vector from the easy axis. To see this, consider the situation when  $\theta = 180^\circ$ . We get:

$$\phi(t) = \tan^{-1} \left( \frac{\alpha h_y(t) + h_x(t)}{h_y(t) - \alpha h_x(t)} \right), \quad (13)$$

$$\theta'(t) = -|\gamma| \frac{h_x^2(t) + h_y^2(t)}{\sqrt{(h_y(t) - \alpha h_x(t))^2 + (\alpha h_y(t) + h_x(t))^2}}. \quad (14)$$

We can see clearly from the above equation that thermal torque can deflect the magnetization from the easy axis since the time rate of change of  $\theta(t)$  [i.e.,  $\theta'(t)$ ] is non-zero in the presence of the thermal field. Note that the initial deflection from the easy axis due to the thermal torque does not depend on the component of the random thermal field along the  $z$ -axis, i.e.,  $h_z(t)$ , which is a consequence of having  $\pm z$ -axis as the easy axes of the nanomagnet. However, once the magnetization direction is even slightly deflected from the easy axis, all three components of the random thermal field along the  $x$ -,  $y$ -, and  $z$ -direction would come into play and affect the deflection.

### C. Thermal distribution of the initial orientation of the magnetization vector

The thermal distributions of  $\theta$  and  $\phi$  in the unstressed magnet are found by solving the Equations (11) and (12)

while setting  $B_{stress} = 0$ . This will yield the distribution of the magnetization vector's initial orientation when stress is turned on. The  $\theta$ -distribution is Boltzmann peaked at  $\theta = 0^\circ$  or  $180^\circ$ , while the  $\phi$ -distribution is Gaussian peaked at  $\phi = \pm 90^\circ$  (Ref. [18]). Since the most probable value of  $\theta$  is either  $0^\circ$  or  $180^\circ$ , where stress is ineffective (*stagnation point*), there are long tails in the switching delay distribution. They are due to the fact that when we start out from  $\theta = 0^\circ, 180^\circ$ , we have to wait a while before thermal kick sets the switching in motion. Thus, switching trajectories initiating from a stagnation point are very slow<sup>19,20</sup>.

In order to eliminate the long tails in the switching delay distribution and thus decrease the mean switching delay, one can apply a small static bias magnetic field that will shift the peak of  $\theta_{initial}$  distribution away from the easy axis, so that the most probable starting orientation will no longer be a stagnation point. This field is applied along the out-of-plane hard axis ( $+x$ -direction) so that the potential energy due to the applied magnetic field becomes  $E_{mag}(t) = -M_V H \sin\theta(t) \cos\phi(t)$ , where  $H$  is the magnitude of magnetic field. The torque generated due to this field is  $\mathbf{T}_M(t) = -\mathbf{n}_m(t) \times \nabla E_{mag}(\theta(t), \phi(t))$ . The presence of this field will modify Equations (11) and (12) to

$$(1 + \alpha^2) \frac{d\theta(t)}{dt} = \frac{|\gamma|}{M_V} [B_{0e}(t) \sin\theta(t) - 2\alpha B(t) \sin\theta(t) \cos\theta(t) + \alpha M_V H \cos\theta(t) \cos\phi(t) - M_V H \sin\phi(t) + (\alpha P_\theta + P_\phi)], \quad (15)$$

$$(1 + \alpha^2) \frac{d\phi(t)}{dt} = \frac{|\gamma|}{M_V} [\alpha B_{0e}(t) + 2B(t) \cos\theta(t) - \sin^{-1}\theta(t) (M_V H \cos\theta(t) \cos\phi(t) + \alpha M_V H \sin\phi(t)) - \sin^{-1}\theta(t) (P_\theta - \alpha P_\phi)]. \quad (\sin\theta \neq 0.) \quad (16)$$

The bias field also makes the potential energy profile of the magnet asymmetric in  $\phi$ -space and the energy minimum will be shifted from  $\phi_{min} = \pm 90^\circ$  (the plane of the magnet) to

$$\phi_{min} = \cos^{-1} \left[ \frac{H}{M_s (N_{d-xx} - N_{d-yy})} \right]. \quad (17)$$

However, the profile will remain symmetric in  $\theta$ -space, with  $\theta = 0^\circ$  and  $\theta = 180^\circ$  remaining as the minimum energy locations. With the parameters used in this paper, a bias magnetic field of flux density 40 mT would make  $\phi_{min} \simeq 87^\circ$ . Application of the bias magnetic field will also reduce the in-plane shape anisotropy energy barrier from 44  $kT$  to 36  $kT$  at room temperature. We assume that a permanent magnet will be employed to produce the bias field and thus will not affect the energy dissipated during switching.

## D. Energy Dissipation

The energy dissipated during switching has two components: (1) the energy dissipated in the switching circuit that applies the stress on the nanomagnet by generating a voltage, and (2) the energy dissipated internally in the nanomagnet because of Gilbert damping. We will term the first component ‘ $CV^2$ ’ dissipation, where  $C$  and  $V$  denote the capacitance of the piezoelectric layer and the applied voltage, respectively. If the voltage is turned on or off abruptly, i.e. the ramp rate is infinite, then the energy dissipated during either turn on or turn off is  $(1/2)CV^2$ . However, if the ramp rate is finite, then this energy is reduced and its exact value will depend on the ramp duration or ramp rate. We calculate it following the same procedure described in Ref. [4]. The second component, which is the internal energy dissipation  $E_d$ , is given by the expression  $\int_0^\tau P_d(t)dt$ , where  $\tau$  is the switching delay and  $P_d(t)$  is the power dissipated during switching<sup>21,22</sup>

$$P_d(t) = \frac{\alpha|\gamma|}{(1+\alpha^2)M_V} |\mathbf{T}_E(t) + \mathbf{T}_M(t)|^2. \quad (18)$$

We sum up the power  $P_d(t)$  dissipated during the entire switching period to get the corresponding energy dissipation  $E_d$  and add that to the ‘ $CV^2$ ’ dissipation in the switching circuit to find the total dissipation  $E_{total}$ . The average power dissipated during switching is simply  $E_d/\tau$ .

There is no net dissipation due to random thermal torque since the mean of the random thermal field is zero. However, that does not mean that the temperature has no effect on either  $E_d$  or the ‘ $CV^2$ ’ dissipation. It affects  $E_d$  since it raises the critical stress needed to switch with non-zero probability and it also affects the stress needed to switch with a given probability. Furthermore, it affects ‘ $CV^2$ ’ because  $V$  must exceed the thermal noise voltage<sup>23</sup> to prevent random switching due to noise. In other words, we must enforce  $CV^2 > kT$ . For the estimated capacitance of our structure (2.6 fF), this translates to  $V > 1.3$  mV.

## III. SIMULATION RESULTS AND DISCUSSIONS

In our simulations, we consider the magnetostrictive layer to be made of polycrystalline Terfenol-D that has the following material properties – Young’s modulus ( $Y$ ):  $8 \times 10^{10}$  Pa, magnetostrictive coefficient ( $(3/2)\lambda_s$ ):  $+90 \times 10^{-5}$ , saturation magnetization ( $M_s$ ):  $8 \times 10^5$  A/m, and Gilbert’s damping constant ( $\alpha$ ): 0.1 (Refs. [24–27]). For the piezoelectric layer, we use lead-zirconate-titanate (PZT), which has a dielectric constant of 1000. The PZT layer is assumed to be four times thicker than the magnetostrictive layer so that any strain generated in it is transferred almost completely to the magnetostrictive layer<sup>3</sup>. We will assume that the maximum strain that can be

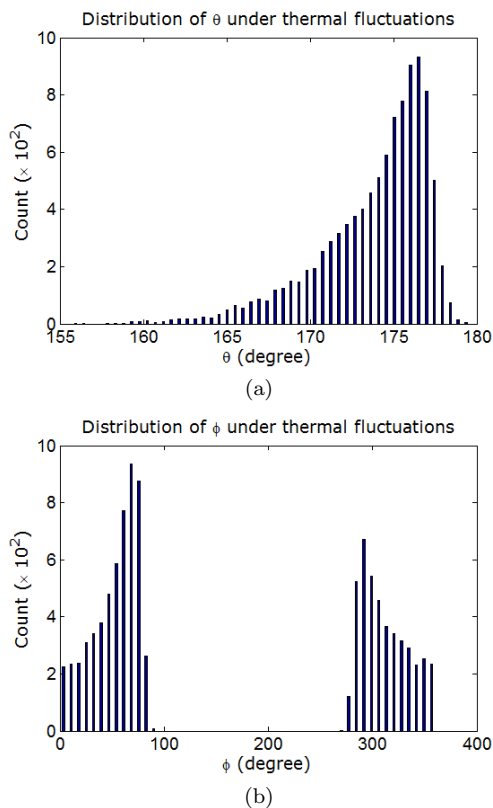


FIG. 2. Distribution of polar angle  $\theta_{initial}$  and azimuthal angle  $\phi_{initial}$  due to thermal fluctuations at room temperature (300 K) when a magnetic field of flux density 40 mT is applied along the out-of-plane hard axis (+ $x$ -direction). (a) Distribution of polar angle  $\theta_{initial}$  at room temperature (300 K). The mean of the distribution is  $173.7^\circ$ , and the most likely value is  $175.8^\circ$ . (b) Distribution of the azimuthal angle  $\phi_{initial}$  due to thermal fluctuations at room temperature (300 K). There are two distributions with peaks centered at  $\sim 65^\circ$  and  $\sim 295^\circ$ .

generated in the PZT layer is 500 ppm<sup>28</sup>, which would require a voltage of 111 mV because  $d_{31}=1.8 \times 10^{-10}$  m/V for PZT<sup>29</sup>. The corresponding stress is the product of the generated strain ( $500 \times 10^{-6}$ ) and the Young’s modulus of the magnetostrictive layer. Hence, 40 MPa is the maximum magnitude of stress that can be generated on the nanomagnet.

We assume that when stress is applied to initiate switching, the magnetization vector starts out from near the south pole ( $\theta \simeq 180^\circ$ ) with a certain  $(\theta_{initial}, \phi_{initial})$  picked from the initial angle distributions at the given temperature. Stress is ramped up linearly and kept constant until the magnetization reaches the plane defined by the in-plane and the out-of-plane hard axis (i.e. the  $x$ - $y$  plane,  $\theta = 90^\circ$ ). This plane is always reached sooner or later since the energy minimum of the stressed magnet in  $\theta$ -space is at  $\theta = 90^\circ$ . Thermal fluctuations can introduce a spread in the time it takes to reach the  $x$ - $y$  plane but cannot prevent the magnetization from reaching it ultimately if the stress is so large that the energy minimum at  $\theta = 90^\circ$  is more than a few  $kT$  deep.

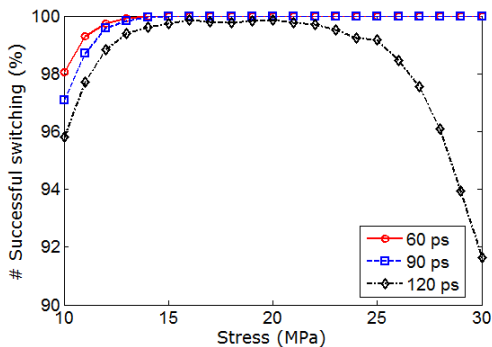


FIG. 3. Percentage of successful switching events among the simulated switching trajectories (or the switching probability) at room temperature in a Terfenol-D/PZT multiferroic nanomagnet when subjected to stress between 10 MPa and 30 MPa. The stress at which switching becomes  $\sim 100\%$  successful increases with ramp duration. For large ramp duration (120 ps) or slow ramp rate,  $\sim 100\%$  switching probability is unachievable.

As soon as the magnetization reaches the  $x$ - $y$  plane, the stress is ramped down at the same rate at which it was ramped up, and reversed in magnitude to facilitate switching. The magnetization dynamics ensures that  $\theta$  continues to rotate towards  $0^\circ$  with very high probability. When  $\theta$  becomes  $\leq 5^\circ$ , switching is deemed to have completed. A moderately large number (10,000) of simulations, with their corresponding  $(\theta_{initial}, \phi_{initial})$  picked from the initial angle distributions, are performed for each value of stress and ramp duration to generate the simulation results in this paper.

Fig. 2 shows the distributions of initial angles  $\theta_{initial}$  and  $\phi_{initial}$  in the presence of thermal fluctuations and an applied bias magnetic field along the  $+x$ -direction. The latter has shifted the peak from the easy axis ( $\theta = 180^\circ$ ). In Fig. 2(b), the  $\phi_{initial}$  distribution has two peaks and resides mostly within the interval  $[-90^\circ, +90^\circ]$  since the bias magnetic field is applied in the  $+x$ -direction. Because the magnetization vector starts out from near the south pole ( $\theta \simeq 180^\circ$ ) when stress is turned on, the effective torque on the magnetization  $-|\gamma|/(1 + \alpha^2) \mathbf{M} \times \mathbf{H}$  due to the  $+x$ -directed magnetic field is such that the magnetization prefers the  $\phi$ -quadrant ( $0^\circ, 90^\circ$ ) slightly over the  $\phi$ -quadrant ( $270^\circ, 360^\circ$ ), which is the reason for the asymmetry in the two distributions of  $\phi_{initial}$ . Consequently, when the magnetization vector starts out from  $\theta \simeq 180^\circ$ , the initial azimuthal angle  $\phi_{initial}$  is a little more likely to be in the quadrant ( $0^\circ, 90^\circ$ ) than the quadrant ( $270^\circ, 360^\circ$ ).

Fig. 3 shows the switching probability as a function of stress for different ramp durations (60 ps, 90 ps, 120 ps) at room temperature (300 K). The minimum stress needed to switch the magnetization with  $\sim 100\%$  probability at 0 K is  $\sim 5$  MPa, but at 300 K, it increases to  $\sim 14$  MPa for 60 ps ramp duration and  $\sim 17$  MPa for 90 ps ramp duration. At low stress levels, the switching prob-

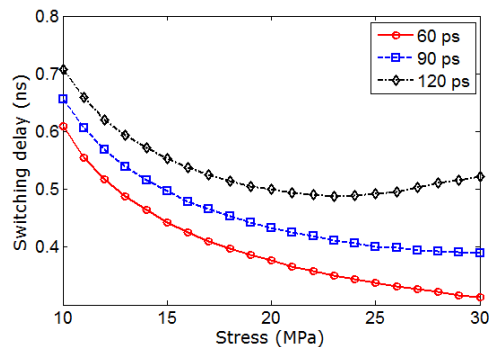


FIG. 4. The thermal mean of the switching delay (at 300 K) versus stress (10-30 MPa) for different ramp durations (60 ps, 90 ps, 120 ps). Switching may fail at low stress levels and also at high stress levels for long ramp durations. Failed attempts are excluded when computing the mean.

ability increases with stress, regardless of the ramp rate. This happens because a higher stress mitigates the detrimental effects of thermal fluctuations more when magnetization reaches the  $x$ - $y$  plane and thus conducive to more success rate of switching. This feature is independent of the ramp rate.

Once the magnetization vector crosses the  $x$ - $y$  plane (i.e. in the second half of switching), the ramp rate becomes important. Now, the stress initially applied to cause switching becomes harmful and impedes switching. That happens because it causes the energy minimum to be located at  $\theta = 90^\circ$ , which will make the magnetization backtrack towards this location during the second half. This is why stress must be removed or reversed immediately upon crossing the  $x$ - $y$  plane so that the energy minimum quickly moves back to  $\theta = 0^\circ, 180^\circ$ , and the magnetization vector rotates towards  $\theta = 0^\circ$ . If the removal rate is fast, then the success probability remains high since the harmful stress does not stay active long enough to cause significant backtracking. However, if the ramp rate is too slow, then significant backtracking occurs whereupon the magnetization vector returns to the  $x$ - $y$  plane and thermal torques can subsequently kick it to the starting position at  $\theta \simeq 180^\circ$ , causing switching failure. That is why the switching probability drops with decreasing ramp rate.

The same effect also explains the non-monotonic stress dependence of the switching probability when the ramp rate is slow. During the first half of the switching, when  $\theta$  is in the quadrant  $[180^\circ, 90^\circ]$ , a higher stress is helpful since it provides a larger torque to move towards the  $x$ - $y$  plane, but during the second half, when  $\theta$  is in the quadrant  $[90^\circ, 0^\circ]$ , a higher stress is harmful since it increases the chance of backtracking. These two counteracting effects are the reason for the non-monotonic dependence of the success probability on stress in the case of the slowest ramp rate.

Fig. 4 shows the thermally averaged switching delay versus stress for different ramp durations. Only success-

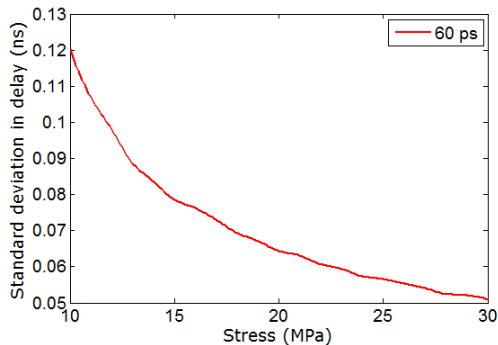


FIG. 5. The standard deviations in switching delay versus stress (10-30 MPa) for 60 ps ramp duration at 300 K. We consider only the successful switching events in determining the standard deviations. The standard deviations in switching delay for other ramp durations are of similar magnitudes and show similar trends.

ful switching events are counted here since the switching delay will be infinity for an unsuccessful event. For a given stress, decreasing the ramp duration (or increasing the ramp rate) decreases the switching delay because the stress reaches its maximum value quicker and hence switches the magnetization faster. For ramp durations of 60 ps and 90 ps, the switching delay decreases with increasing stress since the torque, which rotates the magnetization, increases when stress increases. However, for 120 ps ramp duration, the dependence is non-monotonic, because of the same reasons that caused the non-monotonicity in Fig. 3. Too high a stress is harmful during the second half of the switching since it increases the chances of backtracking. Even if backtracking can be overcome and successful switching ultimately takes place, temporary backtracking still increases the switching delay.

Fig. 5 shows the standard deviation in switching delay versus stress for 60 ps ramp duration. At higher values of stress, the torque due to stress dominates over the random thermal torque that causes the spread in the switching delay. That makes the distribution more peaked as we increase the stress.

Fig. 6 shows the thermal mean of the total energy dissipated to switch the magnetization as a function of stress for different ramp durations. The average power dissipation ( $E_{total}/\tau$ ) increases with stress for a given ramp duration and decreases with increasing ramp duration for a given stress. More stress requires more ‘ $CV^2$ ’ dissipation and also more internal dissipation because it results in a higher torque. Slower switching decreases the power dissipation since it makes the switching more adiabatic. However, since the switching delay curves show the opposite trend (see Fig. 4), the energy dissipation curves in Fig. 6 exhibit the cross-overs.

Fig. 7 shows the ‘ $CV^2$ ’ energy dissipation in the switching circuitry versus stress. Increasing stress requires increasing the voltage  $V$ , which is why the ‘ $CV^2$ ’ energy

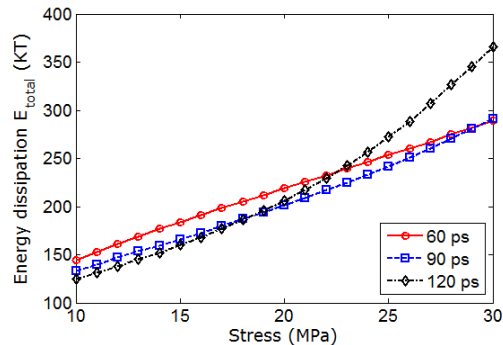


FIG. 6. Thermal mean of the total energy dissipation versus stress (10-30 MPa) for different ramp durations (60 ps, 90 ps, 120 ps). Once again, failed switching attempts are excluded when computing the mean.

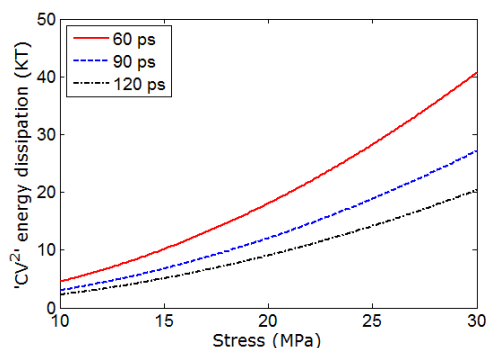


FIG. 7. The ‘ $CV^2$ ’ energy dissipation in the external circuit as a function of stress for different ramp durations.

dissipation increases rapidly with stress. This dissipation however is a small fraction of the total energy dissipation ( $< 15\%$ ) since a very small voltage is required to switch the magnetization of a multiferroic nanomagnet with stress. The ‘ $CV^2$ ’ dissipation decreases when the ramp duration increases because then the switching becomes more ‘adiabatic’ and hence less dissipative. This component of the energy dissipation would have been several orders of magnitude higher had we switched the magnetization with an external magnetic field<sup>30</sup> or spin-transfer torque<sup>11</sup>.

Fig. 8 shows the delay and energy distributions in the presence of room-temperature thermal fluctuations for 15 MPa stress and 60 ps ramp duration. The high-delay tail in Fig. 8(a) is associated with those switching trajectories that start very close to  $\theta = 180^\circ$  which is a stagnation point. In such trajectories, the starting torque is vanishingly small, which makes the switching sluggish at the beginning. During this time, switching also becomes susceptible to backtracking because of thermal fluctuations, which increases the delay further. Since the energy dissipation is the product of the mean power dissipation and the switching delay, similar behavior is found in Fig. 8(b).

Fig. 9 shows two examples of switching dynamics when

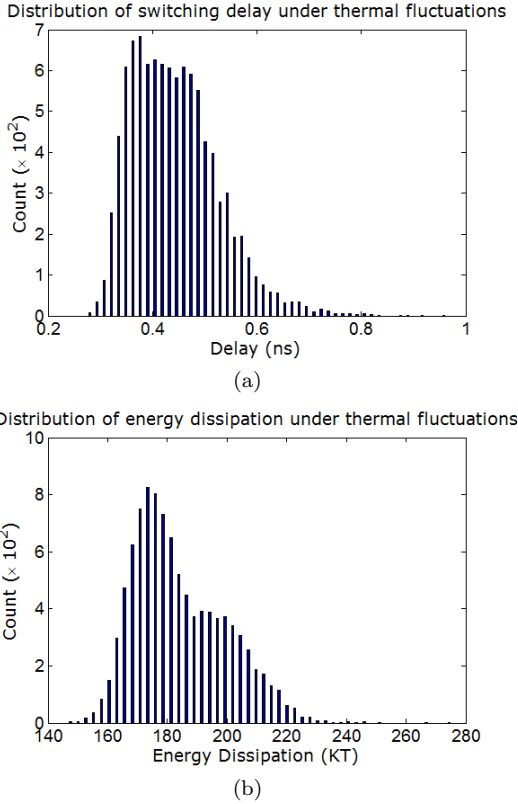


FIG. 8. Delay and energy distributions for 15 MPa applied stress and 60 ps ramp duration at room temperature (300 K). (a) Distribution of the switching delay. The mean and standard deviation of the distribution are 0.44 ns and 83 ps, respectively. (d) Distribution of energy dissipation. The mean and standard deviation of the distribution are 184  $kT$  and 15.5  $kT$  at room temperature, respectively.

the applied stress is 10 MPa and the ramp duration is 60 ps. In Fig. 9(a), magnetization switches successfully. Thermal fluctuations cause the ripples because of temporary backtracking but  $\theta$  switches from  $\sim 180^\circ$  to  $\sim 0^\circ$  finally. Note that despite appearances,  $\phi$  is not changing discretely. When it crosses  $360^\circ$ , it re-enters the quadrant  $[0^\circ, 90^\circ]$ , which is why it appears as if there is a discrete jump in the value of  $\phi$  in Fig. 9. On the other hand, Fig. 9(b) shows a failed switching dynamic. Here, the magnetization backtracks towards  $\theta = 180^\circ$  and settles close to that location, thus failing in its attempt to switch. This happened because of the coupled  $\theta$ - $\phi$  dynamics that resulted in a misdirected torque when the magnetization reached the  $x$ - $y$  plane. This kind of dynamics has been explained in Ref. 18.

#### IV. CONCLUSIONS

We have theoretically investigated stress-induced switching of multiferroic nanomagnets in the presence of thermal fluctuations. The room-temperature thermal

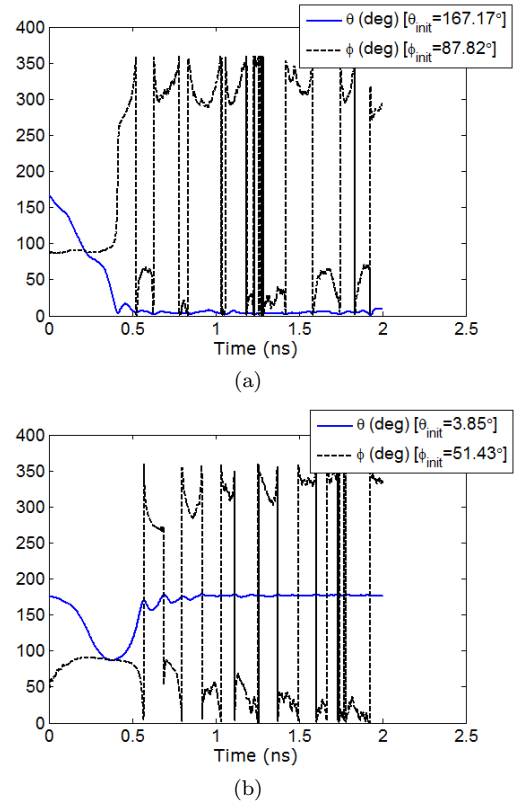


FIG. 9. Temporal evolution of the polar angle  $\theta(t)$  and azimuthal angle  $\phi(t)$  for 10 MPa applied stress and 60 ps ramp duration. Simulations are carried out for room temperature (300 K). (a) Magnetization switches successfully. (b) Magnetization fails to switch and backtracks towards the initial state.

average of the energy dissipation is as small as  $\sim 200$   $kT$  while the thermal average of the switching delay is  $\sim 0.5$  ns with a standard deviation less than 0.1 ns. This makes strain-switched multiferroic nanomagnets very attractive platforms for implementing non-volatile memory and logic systems because they are minimally dissipative while being adequately fast. Our results also show that a certain critical stress is required to switch with  $\sim 100\%$  probability in the presence of thermal noise. The value of this critical stress increases with decreasing ramp rate until the ramp rate becomes so slow that  $\sim 100\%$  switching probability becomes unachievable. Thus, a faster ramp rate is beneficial. The energy dissipations and switching delays are roughly independent of ramp rate if switching is always performed with the critical stress.

This work was supported by the US National Science Foundation under Nanoelectronics for the year 2020 grant ECCS-1124714 and by the Semiconductor Research Corporation under the Nanoelectronics Research Initiative.

<sup>1</sup>W. Eerenstein, N. D. Mathur, and J. F. Scott, Nature **442**, 759 (2006).

- <sup>2</sup>C. W. Nan, M. I. Bichurin, S. Dong, D. Viehland, and G. Srinivasan, *J. Appl. Phys.* **103**, 031101 (2008).
- <sup>3</sup>K. Roy, S. Bandyopadhyay, and J. Atulasimha, *Appl. Phys. Lett.* **99**, 063108 (2011).
- <sup>4</sup>K. Roy, S. Bandyopadhyay, and J. Atulasimha, *Phys. Rev. B* **83**, 224412 (2011).
- <sup>5</sup>J. Atulasimha and S. Bandyopadhyay, *Appl. Phys. Lett.* **97**, 1 (2010).
- <sup>6</sup>M. S. Fashami, K. Roy, J. Atulasimha, and S. Bandyopadhyay, *Nanotechnology* **22**, 155201 (2011).
- <sup>7</sup>N. D'Souza, J. Atulasimha, and S. Bandyopadhyay, *J. Phys. D: Appl. Phys.* **44**, 265001 (2011).
- <sup>8</sup>T. Brintlinger, S. H. Lim, K. H. Baloch, P. Alexander, Y. Qi, J. Barry, J. Melngailis, L. Salamanca-Riba, I. Takeuchi, and J. Cumings, *Nano Lett.* **10**, 1219 (2010).
- <sup>9</sup>T. L. Gilbert, *IEEE Trans. Magn.* **40**, 3443 (2004).
- <sup>10</sup>W. F. Brown, *Phys. Rev.* **130**, 1677 (1963).
- <sup>11</sup>J. Z. Sun, *Phys. Rev. B* **62**, 570 (2000).
- <sup>12</sup>S. Mark, P. Durrenfeld, K. Pappert, L. Ebel, K. Brunner, C. Gould, and L. W. Molenkamp, *Phys. Rev. Lett.* **106**, 57204 (2011).
- <sup>13</sup>B. Behin-Aein, D. Datta, S. Salahuddin, and S. Datta, *Nature Nanotechnol.* **5**, 266 (2010).
- <sup>14</sup>S. Chikazumi, *Physics of Magnetism* (Wiley New York, 1964).
- <sup>15</sup>M. Beleggia, M. D. Graef, Y. T. Millev, D. A. Goode, and G. E. Rowlands, *J. Phys. D: Appl. Phys.* **38**, 3333 (2005).
- <sup>16</sup>R. P. Cowburn, D. K. Koltsov, A. O. Adeyeye, M. E. Welland, and D. M. Tricker, *Phys. Rev. Lett.* **83**, 1042 (1999).
- <sup>17</sup>G. Brown, M. A. Novotny, and P. A. Rikvold, *Phys. Rev. B* **64**, 134422 (2001).
- <sup>18</sup>K. Roy, S. Bandyopadhyay, and J. Atulasimha, arXiv:1111.5390 (2011).
- <sup>19</sup>A. Brataas, G. E. W. Bauer, and P. J. Kelly, *Phys. Rep.* **427**, 157 (2006).
- <sup>20</sup>Z. Z. Sun and X. R. Wang, *Phys. Rev. B* **73**, 092416 (2006).
- <sup>21</sup>Z. Z. Sun and X. R. Wang, *Phys. Rev. B* **71**, 174430 (2005).
- <sup>22</sup>B. Behin-Aein, S. Salahuddin, and S. Datta, *IEEE Trans. Nanotech.* **8**, 505 (2009).
- <sup>23</sup>L. B. Kish, *Phys. Lett. A* **305**, 144 (2002).
- <sup>24</sup>R. Abbundi and A. E. Clark, *IEEE Trans. Magn.* **13**, 1519 (1977).
- <sup>25</sup>K. Ried, M. Schnell, F. Schatz, M. Hirscher, B. Ludescher, W. Sigle, and H. Kronmüller, *Phys. Stat. Sol. (a)* **167**, 195 (1998).
- <sup>26</sup>R. Kellogg and A. Flatau, *J. Intell. Mater. Sys. Struc.* **19**, 583 (2008).
- <sup>27</sup><http://www.allmeasures.com/Formulae/static/materials/>.
- <sup>28</sup>M. Lisca, L. Pintilie, M. Alexe, and C. M. Teodorescu, *Appl. Surf. Sci.* **252**, 4549 (2006).
- <sup>29</sup><http://www.memsnets.org/material/leadzirconatetitanatepzt/>.
- <sup>30</sup>M. T. Alam, M. J. Siddiq, G. H. Bernstein, M. T. Niemier, W. Porod, and X. S. Hu, *IEEE Trans. Nanotech.* **9**, 348 (2010).